Nonadiabatic Effects in the Photodissociation and Electronic Spectroscopy of $HMn(CO)_3(dab)$: Quantum Wave Packet Dynamics Based on *ab Initio* Potentials

K. Finger,*,† C. Daniel,‡ P. Saalfrank,† and B. Schmidt†

Institut für Physikalische und Theoretische Chemie, Freie Universität Berlin, Takustrasse 3, D-14195 Berlin, Germany, and Laboratoire de Chimie Quantique, UPR 139 du CNRS, Université Louis Pasteur, 67000 Strasbourg, France

Received: August 25, 1995; In Final Form: October 31, 1995[X]

The photochemistry of many transition metal complexes is governed by a multitude of electronically excited states, coupled by various mechanisms. For the transition metal complex $HMn(CO)_3(dab)$ (dab = 1,4-diaza-1,3-butadiene) the photoreactivity (cleavage of the Mn−H bond) and electronic absorption spectra are characterized on the basis of quantum mechanical first-principles calculations. In a first step, the A′ ground (singlet) and the three lowest electronically excited (triplet) potential curves along the Mn−H bond distance are computed using the CASSCF/CCI method. Two of the excited states are found to be bound and are of the metal-to-ligand charge transfer type, whereas the third, ligand-to-ligand charge transfer state is repulsive. In the relevant energy region, two avoided crossings are observed, indicative for strong nonadiabatic couplings. In a second step, the UV/vis photochemistry of the complex is investigated by means of nuclear wave packet dynamics. We solve the nonadiabatically coupled, time-dependent Schrödinger equation in a diabatic representation for different initial conditions to determine both photodissociation yields and electronic absorption spectra. In particular, the effect of the nonadiabatic couplings on the electronic absorption spectrum and on the photoreactivity is investigated.

I. Introduction

The photochemistry and photophysics of many organometallic compounds with low-lying, long-lived metal-to-ligand charge transfer (MLCT) states have found considerable interest, mostly because these molecules appear to be good photosensitizers for photoenergy and photoelectron transfer.[1−9] In particular, $Ru(bpy)_3^{2+}$ (bpy = 2,2′-bipyridine), with favorable oxidation and reduction potentials and a long lifetime of its lowest MLCT state, was extensively studied as a sensitizer for the photolysis of water.[1]

Until recently, the nonreactivity and the long lifetime of the MLCT states of these compounds were considered as characteristics for all transition organometallics. Meanwhile, however, for a family of α-diimine mono- and dinuclear transition metal carbonyls,[10−14] two different kinds of response after irradiation into the MLCT band were experimentally observed. Depending on the metal, on the diimine ligand, and on other experimental conditions (temperature, solvent), the diimines either show stimulated emission or undergo ligand dissociation. These different, "spectroscopic" or "reactive", channels may be useful to promote various applications, such as energy transfer processes or the formation of reactive intermediates used in substitution reactions and catalytic processes. A fundamental question concerns the microscopic functioning of the MLCT states and its dependence on the metal center, the ligands, and the external experimental conditions.

From a theoretical point of view, one way for getting insight into the nature of the photoexcited states involved in the photochemistry of these molecules is to calculate the electronic excitation energies and to determine the corresponding potential energy surfaces for the observed primary reactions.[15−18] In a second step, time-dependent quantum wave packet propagation methods can be used to characterize the photodissociation dynamics.[19−22] Additionally, the time-dependent wave packet approach may also be employed to calculate electronic emission or absorption spectra.[23,24]

For the model diimine complex $HMn(CO)_3(dab)$ (dab = 1,4-diaza-1,3-butadiene), we have speculated in a recent work[25] on the basis of the potential energy curves (PECs) computed for the metal−hydrogen bond cleavage reaction that an unbound ^{3}LLCT (ligand-to-ligand charge transfer) ($\sigma \rightarrow \pi^*$) excited state might be responsible for the metal−hydrogen bond homolysis. (σ and π stand for Mn−H bonding and diimine ligand bonding orbitals, respectively. σ^* and π^* are the corresponding antibonding orbitals.) This dissociative state exhibits two avoided crossings with two low-lying, bound MLCT states of $d \rightarrow \pi^*$ character. (d denotes a Mn 3d atomic orbital.) Therefore, the MLCT states are expected to be strongly nonadiabatically coupled to the repulsive state, this way giving a possible explanation for the observed photoreactivity of the MLCT excited educts.

There is a growing industry focusing on the role played by nonadiabatic effects for (different) molecular dynamics problems. On the quantum chemistry side, nonadiabatic couplings have found much attention.[26−32] There are not as many studies concerning the nuclear motion on nonadiabatically coupled surfaces and the influence of the coupling on the general dynamics,[33,34−36] on electronic spectra,[27,37,38] or on the photoreactivity.[39]

The aim of this work is to contributes on a first-principles basiss to the microscopic understanding of the photoreactivity and the spectroscopy of transition metal diimine complexes. In particular, for the model system $HMn(CO)_3(dab)$ the influence of the nonadiabatic couplings between various excited states on the UV/vis-induced photoreactivity (homolysis of the Mn−H bond) and electronic spectroscopy (here, absorption spectra) is considered in some detail.

The complete treatment of the photochemistry and photophysics of $HMn(CO)_3(dab)$ based on first principles is an

† Freie Universität Berlin.
‡ Université Louis Pasteur.
[X] Abstract published in *Advance ACS Abstracts,* February 1, 1996.

0022-3654/96/20100-3368$12.00/0 © 1996 American Chemical Society

extremely formidable task. To simplify the problem, we first restrict ourselves to the one-dimensional model referred to earlier (with the Mn−H distance z being the only degree of freedom considered). The second simplification concerns the excited state dynamics. The electronic ground state of $HMn(CO)_3(dab)$ is known to be a singlet, whereas the (low-energy) photolysis products of similar diimine complexes form triplets. A working hypothesis, based on earlier work on similar complexes,[21] explains these findings on the photoreactivity with (i) an initial UV excitation of the complex to the singlet manifold of MLCT states, (ii) subsequent fast intersystem crossing (ISC) to the triplet MLCT manifold due to spin−orbit coupling, and (iii) finally "reaction", *i.e.* Mn−H bond cleavage due to nonadiabatic coupling of the ^{3}MLCT states to the repulsive ^{3}LLCT state. Since here we are mostly interested in non-adiabatic, and not in spin−orbit coupling, effects and since the calculation of the excited singlets is still under work, we further restrict the study to excited triplet states (of A′ symmetry) and take solely non-adiabatic couplings into account. Also, the exciting continuous wave laser is never explicitly included. Rather, the singlet ground state is employed to compute initial states for the excited triplet state dynamics, taken as a crude model for the "distorted" initial wave packets resulting from the initial excitation, and the subsequent ISC. Electronic spectroscopy is handled in a similarly simplified manner. Accordingly, absorption spectra are computed by projecting the singlet ground state wave function in Condon approximation on the excited triplet manifold. The subsequent time evolution leads to a wave packet autocorrelation function, which can be used to generate the absorption spectrum.[23] The real (spin-allowed) absorption spectrum, of course, is a result of the complicated three-step scenario just described. However, (i) if the spin−orbit coupling is rapid, as compared to the subsequent dynamics on the triplet states, and (ii) if the initial singlet ↠ singlet absorption is resonant at an energy similar to that of the hypothetical singlet ↠ triplet transition, then our approximate spectrum should be a good representative for the real spectrum. The latter, however, should show a broad structureless background due to the preceding rapid intersystem crossing. The hypothesis of fast intersystem crossing for complexes similar to the one studied here has in fact been supported theoretically in ref 21 and experimentally in ref 40.

This paper is organized as follows. In section II we summarize the general aspects of the time-dependent nuclear dynamics approach used here. In particular, the notion of diabatic and adiabatic representations for the time-dependent Schrödinger equation and the transformation between both "pictures" is recapitulated. In section III.A the model compound $HMn(CO)_3(dab)$ is introduced, and details on the *ab initio* calculation of the (adiabatic) potentials are given. The excited state nuclear dynamics calculations will be performed in the more convenient diabatic representation. Therefore, in section III.B a diabatization procedure for $HMn(CO)_3(dab)$ is described. In section III.C details of the excited state wave packet propagation are summarized. In section IV several results are presented. In section IV.A we roughly characterize the photo-induced dynamics in $HMn(CO)_3(dab)$ by means of wave packet "snapshots" for two different initial conditions, corresponding to two different excitation energies (33 000 and 20 000 cm^{-1}, respectively). The dynamics is further classified as "diabatic" or "adiabatic", respectively. In section IV.B electronic absorption spectra are computed as described above. By artificially leaving several of the excited state couplings out, the influence of non-adiabatic corrections on the spectra is systematically addressed. The same proceedings serve to study the effects of non-adiabatic couplings on the photoreactivity of $HMn(CO)_3(dab)$ in section IV.C. Here, also the possibility to increase photodissociation yields by applying the concept of "vibrationally mediated photochemistry" is investigated. Section V concludes our work.

II. Theory: Adiabatic and Diabatic Dynamics

The investigation of the time evolution of our model requires the solution of the time-dependent Schrödinger equation, which can be written either in the diabatic or in the adiabatic representation.

The time-dependent Schrödinger equation in the *adiabatic* representation is

$$i\hbar\frac{\partial}{\partial t}\underline{\chi}^a = \underline{\underline{\hat{H}}}^a\underline{\chi}^a \tag{2.1}$$

$\underline{\chi}^a$ is a vector containing the individual adiabatic nuclear wave functions χ_i^a, moving under the influence of the adiabatic Hamiltonian matrix operator $\underline{\underline{\hat{H}}}^a$. Explicitly, the time-dependence of χ_i^a is given by

$$i\hbar\frac{\partial}{\partial t}\chi_i^a = [V_{ii}^a + \hat{T}_n + \hat{K}_{ii}]\chi_i^a + \sum_{j\neq i}^{F}\hat{K}_{ij}\chi_j^a \tag{2.2}$$

Here, $\underline{\underline{V}}^a$ is a diagonal matrix containing the adiabatic potentials V_{ii}^a, F is the number of electronic states, and $\hat{T}_n$ is the nuclear kinetic energy operator.

$$\hat{T}_n = -\frac{\hbar^2}{2\mu}\frac{\partial^2}{\partial z^2} \tag{2.3}$$

with μ being the reduced mass and z the bond distance in a one-dimensional model.

Further, the $\hat{K}_{ij}$ are given by

$$\hat{K}_{ij} = -\frac{\hbar^2}{2\mu}\left[\left\langle\phi_i^a\middle|\frac{\partial^2}{\partial z^2}\phi_j^a\right\rangle + 2\left\langle\phi_i^a\middle|\frac{\partial}{\partial z}\phi_j^a\right\rangle\frac{\partial}{\partial z}\right] \tag{2.4}$$

and are called the *non-Born−Oppenheimer* ($i = j$) or *nonadiabatic kinetic coupling* terms ($i \neq j$), respectively. ϕ_i^a is the adiabatic electronic wave function corresponding to V_{ii}^a, and the $\langle\,\rangle$ in (2.4) denote integrations over all electronic coordinates.

The kinetic couplings in the adiabatic representation are typically sharply peaked around so-called avoided crossings and are, additionally, momentum-dependent. This can cause an instability problem during the numerical solution of the time-dependent Schrödinger equation (2.1). However, by a unitary transformation the kinetic couplings can be forced to vanish.[41] Instead, in this *diabatic* representation the coupling becomes potential-like, varies usually only smoothly with z, and allows therefore for a stable numerical solution of the Schrödinger equation.

It can be shown that the unitary transformation matrix $\underline{\underline{U}}$ has to obey the differential equation[41]

$$\frac{\partial}{\partial z}\underline{\underline{U}} + \underline{\underline{T}}^{(1)}\underline{\underline{U}} = \underline{\underline{0}} \tag{2.5}$$

subject to the boundary conditions

$$\underline{\underline{U}}(z=\infty) = \underline{\underline{1}} \tag{2.6}$$

In (2.5), the $\underline{\underline{T}}^{(1)}$ matrix contains the first derivative part of the

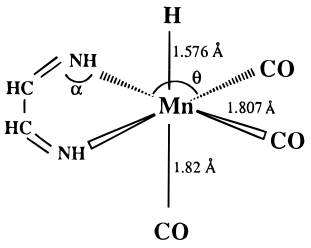

Figure 1. Diimine model molecule $HMn(CO)_3(dab)$ in the C_s conformation. Idealized geometries were deduced from the structures of $Mn(CO)_3(dab)Cl$[54] and $HMn(CO)_5$[55] with $\theta = 96°$ and $\alpha = 117.5°$.

kinetic coupling (2.4) between potential i and j in the adiabatic representation:

$$T_{ij}^{(1)} = \left\langle \phi_i^a \middle| \frac{\partial}{\partial z} \phi_j^a \right\rangle \tag{2.7}$$

If the $T_{ij}^{(1)}$ are known, *e.g.* from *ab initio* calculations, (2.5) can be numerically solved to give $\underline{\underline{U}}$ (see below). The diagonal, adiabatic potential matrix $\underline{\underline{V}}^a$ is then transformed to the diabatic potential matrix $\underline{\underline{V}}^d$ according to

$$\underline{\underline{V}}^d = \underline{\underline{U}}^+ \underline{\underline{V}}^a \underline{\underline{U}} \tag{2.8}$$

Similarly, adiabatic and diabatic nuclear wave functions χ^a and χ^d are interconnected by

$$\chi^d = \underline{\underline{U}}^+ \chi^a \tag{2.9}$$

The transformation leads to the mentioned diabatic representation of the time-dependent Schrödinger equation

$$i\hbar \frac{\partial}{\partial t} \chi^d = \underline{\underline{\hat{H}}}^d \chi^d \tag{2.10}$$

with

$$i\hbar \frac{\partial}{\partial t} \chi_i^d = [V_{ii}^d + \hat{T}_n] \chi_i^d + \sum_{j \neq i}^{F} V_{ij}^d \chi_j^d \tag{2.11}$$

describing the time evolution of the diabatic nuclear wave function χ_i^d on the diabatic potential surface V_{ii}^d, coupled to all $V_{jj}^d (j \neq i)$ through the potential coupling terms V_{ij}^d.

III. Model and Methods

A. *Ab Initio* Potentials. The adiabatic potential energy curves $V_{ii}^a(z)$ for the electronic singlet ground state, and the lowest three triplet excited states of $^3A'$ symmetry of the $HMn(CO)_3(dab)$ complex, have previously been calculated *ab initio* along the Mn−H distance z, using the molecular geometry reported in Figure 1.[25] It was assumed that C_s symmetry is retained along the reaction path corresponding to the homolysis of the metal−hydrogen bond.

Gaussian basis sets roughly of triple-ζ plus polarization functions quality were employed.[25] Complete active space self-consistent-field (CASSCF) calculations[42] were carried out to obtain wave functions, which were then used as references in multireference contracted configuration interaction (CCI) calculations.[43] For each electronic state a separate CASSCF calculation followed by a multireference CI calculation was performed. Eight electrons were correlated (the 3d electrons and the two electrons involved in the Mn−H bond) in 10 active orbitals, corresponding to the 3d and the 4d atomic orbitals of Mn, and the σ, σ^*, and the lowest π^* orbitals (see above). More computational details are reported in ref 25.

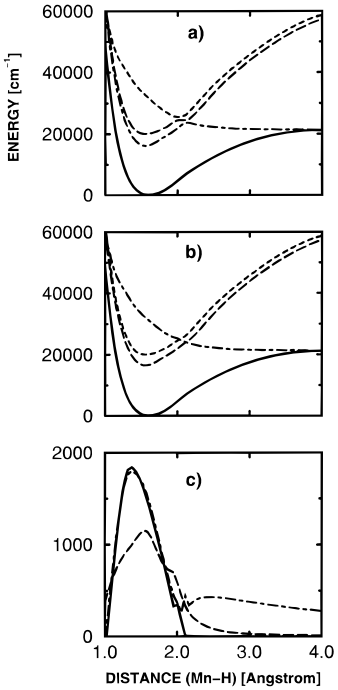

Figure 2. (a) Adiabatic *ab initio* curves for the ground state and the three lowest excited triplet states of A′ symmetry of $HMn(CO)_3(dab)$ along the Mn−H bond distance z, obtained by CASSCF/CCI calculations:[25] $a^1A' = V_{11}^a$ (solid curve), $a^3A' = V_{22}^a$ (dot-dashed curve), $b^3A' = V_{33}^a$ (long-dashed curve), and $c^3A' = V_{44}^a$ (dashed line). The energetically nonaccessible parts of b^3A' and c^3A' beyond 2.5 Å were extrapolated. (b) Diabatic curves obtained from adiabatic *ab initio* potentials: V_{11}^d ground state (solid line), V_{22}^d ^{3}LLCT state with σ → π^* character (dot-dashed line), V_{33}^d ^{3}MLCT state with d_{xz} → π^* character (long-dashed line), and V_{44}^d ^{3}MLCT state with $d_{x^2-y^2}$ → π^* character (dashed line). (c) Excited state potential coupling curves obtained after diabatization of the adiabatic curves: V_{23}^d (dot-dashed curve), V_{24}^d (solid line), and V_{34}^d (dashed line). The potential couplings vary smoothly over z, reaching maxima in the ground state equilibrium region.

The adiabatic potential energy curves corresponding to the a^1A' ground state and the a-, b-, and c^3A' excited states along the Mn−H distance z of the $HMn(CO)_3(dab)$ complex are shown in Figure 2a. The singlet ground state is a bound Morse-type PEC, with the minimum at a Mn−H distance of ca. 1.7 Å and a well depth of ca. 21 000 cm^{-1}. Similarly, two of the three excited triplet potentials are bound, with minima at approximately the same Mn−H distance and ca. 20 000 cm^{-1} above the ground state. These excited PECs are of metal-to-ligand charge transfer (MLCT) character and exhibit two avoided crossings around $z \approx 2.0$ Å with a third, dissociative potential with ligand-to-ligand charge transfer character. The lower MLCT state arises, in one-particle language, from a d_{xz} → π^* excitation, whereas the upper MLCT state is a result of a $d_{x^2-y^2}$ → π^* and the LLCT state is a result of a σ → π^* transition. (Strictly, the characterization of the excited states as "bound" or "dissociative", or as MLCT or LLCT type, and the corresponding assignment of one-particle excitations are valid only for the diabatic potentials, since the character of the adiabatic electronic states changes abruptly around the avoided crossings.) The adiabatic curves shown are generated from the *ab initio* points by interpolation with a cubic spline fit. For the sake of simplicity they are labeled as follows: $a^1A' \equiv V_{11}^a$, $a^3A' \equiv V_{22}^a$, $b^3A' \equiv V_{33}^a$, and $c^3A' \equiv V_{44}^a$.

B. Diabatization Procedure. The diabatic curves are obtained from the adiabatic ones by calculating the transformation matrix $\underline{U}$ and then $\underline{V}^d$ according to (2.5)−(2.8). The algorithm used to solve (2.5) numerically is described in ref 44. Due to the fact that only the three excited potentials are expected to be strongly nonadiabatically coupled, the diabatization procedure is restricted to the excited manifold, leaving the ground state unaltered. In fact, the simulation of the subsequent dynamics is performed only on the three excited states, with the ground state merely serving to provide (approximate) initial wave functions.

The $T_{ij}^{(1)}$ needed in (2.5) can in principle be evaluated by *ab initio* calculations. This involves the tedious numerical differentiation of the electronic CASSCF wave functions. On the other hand, the kinetic couplings are known to be large only around the avoided crossings, where they can safely be approximated by Lorentzians.[45] In the present work, we use asymmetric Lorentzians

$$T_{ij}^{(1)} = \begin{cases} \dfrac{\Gamma_{ij}^l}{4[z - z_{ij}^c]^2 + (\Gamma_{ij}^l)^2} & \dfrac{\Gamma_{ij}^l}{\frac{1}{2}(\Gamma_{ij}^l + \Gamma_{ij}^r)} \quad \text{for } z \leq z_{ij}^c \\ \dfrac{\Gamma_{ij}^r}{4[z - z_{ij}^c]^2 + (\Gamma_{ij}^r)^2} & \dfrac{\Gamma_{ij}^r}{\frac{1}{2}(\Gamma_{ij}^l + \Gamma_{ij}^r)} \quad \text{for } z > z_{ij}^c \end{cases} \tag{3.1}$$

which are normalized to yield an integral of $\pi/2$. Here, Γ_{ij}^l and Γ_{ij}^r are parameters governing the half-width at half-maximum (hwhm) for a bond distance smaller and larger than the location z_{ij}^c of the avoided crossing between state i and j, respectively.

In the following for the excited state kinetic coupling parameters Γ_{ij} and z_{ij}^c we used $\Gamma_{23}^l = \Gamma_{34}^l = 0.037$ Å, $\Gamma_{23}^r = \Gamma_{34}^r = 0.053$ Å, $z_{23}^c = 2.105$ Å, and $z_{34}^c = 2.020$ Å. Since the adiabatic potentials V_{22}^a and V_{44}^a do not avoid a crossing with each other, the kinetic coupling $T_{24}^{(1)}$ was assumed to be zero. The z_{ij}^c were directly taken from the *ab initio* curves, and the criterion for the choice of the Γ_{ij} was the accurate matching of the diabates with the adiabates outside the region of the avoided crossing.

The diabatic curves obtained for $HMn(CO)_3$(dab) are shown in Figure 2b, with the labeling being as follows: $a^1A' \equiv V_{11}^d$, $d_{zz} - \pi^* \equiv V_{33}^d$, $d_{x^2-y^2} - \pi^* \equiv V_{44}^d$, and $\sigma - \pi^* \equiv V_{22}^d$. Note that V_{11}^d is of course identical to V_{11}^a over the whole range, whereas for the other curves $V_{ii}^d = V_{ii}^a$ only holds for $z \to \infty$. Additionally, in Figure 2c the off-diagonal elements of the excited state diabatic potential matrix, *i.e.* the potential couplings, are shown. In contrast to the sharp, Lorentzian kinetic coupling elements $T_{ij}^{(1)}$, the numerically determined V_{ij}^d are found to vary only smoothly with z, showing maxima around the equilibrium region and vanishing for $z \to \infty$ and $z \to 0$.

C. Wave Packet Propagation. The photoabsorption and the Mn−H bond-breaking processes in $HMn(CO)_3$(dab) are simulated here by the propagation of selected wave packets on the excited triplet states according to (2.11). For the excited state dynamics, we use vibrational eigenstates $\chi_{1,v}$ of the singlet ground state as initial states, which are then transferred to the excited triplet states in a Franck−Condon-like manner. As mentioned above, this serves as a crude model for the initial state resulting from photoexcitation plus subsequent, fast intersystem crossing.

The eigenstates of the electronic ground state are obtained by the Fourier grid Hamiltonian method.[47] To systematically study the influence of individual excited potentials and their couplings on the reaction (*i.e.*, the Mn−H bond breaking) or the optical absorption spectrum, we perform propagations on different subsets of excited potentials and with different initial conditions. For instance, occassionally we follow the dynamics using two rather than three coupled excited PECs; that is, one diabatic curve and the corresponding couplings are simply left out (see below).

The time-dependent Schrödinger equation in the diabatic picture is solved on a grid $z_l = z_0 + (l - 1)\Delta z$, with $z_0 = 1.0$ Å, $\Delta z = 0.053$ Å, and $l = 1, 2, ..., 512$. The kinetic energy operator is evaluated locally, using the fast fourier transform (FFT) technique.[48] The time propagation is done by the Chebychev method for long time propagations to obtain well-resolved spectra[49] or by fourth-order differencing (FOD)[33a] to produce snapshots for the wave packet evolution. The discretization in time, $t_j = j\Delta t$, is done with $\Delta t = 0.007\,26$ fs and $j = 1, 2, ..., 28\,000$ for FOD and with $\Delta t = 7.26$ fs and $j = 1, 2, ..., 1320$ for the Chebychev propagation, respectively. To avoid numerical artifacts due to a finite grid, absorbing boundary conditions are used for long time propagations.[50]

IV. Results and Discussion

In our systematic theoretical study of the photoabsorption and Mn−H bond-breaking processes in $HMn(CO)_3$(dab), the time-dependent, diabatically coupled 3 × 3 Schrödinger equation (2.10) is solved subject to the following initial conditions and situations (see Figure 3a−h for illustration):

(a) $\chi_3^d(z,t=0) = \chi_{1,0}(z)$, propagation on three coupled excited potentials V_{ii}^d $(i = 2, 3, 4)$

(b) $\chi_3^d(z,t=0) = \chi_{1,0}(z)$, propagation on two coupled potentials V_{ii}^d $(i = 2, 3)$

(c) $\chi_4^d(z,t=0) = \chi_{1,0}(z)$, propagation on three coupled potentials V_{ii}^d $(i = 2, 3, 4)$

(d) $\chi_4^d(z,t=0) = \chi_{1,0}(z)$, propagation on two coupled potentials V_{ii}^d $(i = 2, 4)$

(e) $\chi_2^d(z,t=0) = \chi_{1,0}(z)$, propagation on three coupled potentials V_{ii}^d $(i = 2, 3, 4)$

(f) $\chi_2^d(z,t=0) = \chi_{1,0}(z)$, propagation on two coupled potentials V_{ii}^d $(i = 2, 3)$

(g) $\chi_2^d(z,t=0) = \chi_{1,0}(z)$, propagation on two coupled potentials V_{ii}^d $(i = 2, 4)$

Further, to study the influence of the initial vibrational excitation on the dissociation probability we also consider

(h) $\chi_3^d(z,t=0) = \chi_{1,v}(z)$, propagation on three coupled potentials V_{ii}^d $(i = 2, 3, 4)$ with $v = 1, ..., 6$

Note that cases a, c, e, and h correspond to at least in principle experimentally realizable situations, whereas the other cases serve as computer experiments, where certain couplings are selectively turned off.

A. Time Evolution of the Wave Packet: Snapshots. To gain a first insight into the time evolution of $HMn(CO)_3$(dab) after photoexcitation, two representative cases are investigated.

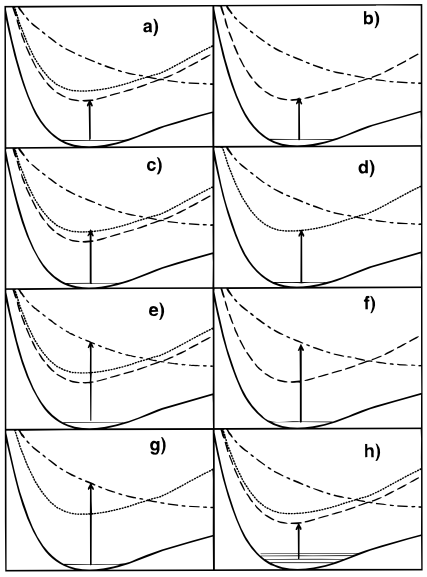

Figure 3. Different excitation and coupling schemes employed in this work to investigate the influence of single potential couplings on the electronic absorption spectrum and the dissociation probability.

In the first case, we consider the initial excitation into the lower bound MLCT state around 20 000 cm^{-1} (case a), whereas in the second case we excite into the LLCT state around 33 000 (case e). Both cases represent typical features in the experimental optical spectra (see below) and are characterized by very distinct dynamics.

The propagation is done in the diabatic picture. For interpretative reasons, however, the diabatic wave packet $\underline{\chi}^d$ is transformed to the adiabatic one at selected times according to

$$\underline{\chi}^a = \underline{\underline{U}}\,\underline{\chi}^d \tag{4.1}$$

Time Evolution on the Lower Bound ^{3}MLCT State (d_{xz} f π^*, V^d_{33}). First, the diabatic time evolution of $HMn(CO)_3$-(dab) following absorption to the lowest ^{1}MLCT excited state and ^{1}MLCT f ^{3}MLCT intersystem crossing is simulated according to (2.10), with the initial conditions $\chi^d_3(z,0) = \chi_{1,0}(z)$ and $\chi^d_2(z,0) = \chi^d_4(z,0) = 0$, taking all three coupled excited states into account (case a). Snapshots of the absolute value of the wave function $|\chi^d_i(z,t)|$ for $i = 2, 3, 4$ at various times t are given in Figure 4a. On an ultrafast time scale (within ca. 5 fs) about 20% of the wave packet is transferred from potential V^d_{33} to the upper bound ^{3}MLCT ($d_{x^2-y^2}$ f π^*) state V^d_{44} and about 1% to the dissociative ^{3}LLCT state V^d_{22}. This is a consequence of the potential couplings shown in Figure 2c. The wave packet on the repulsive PEC V^d_{22} can dissociate, whereas the main part remains trapped and oscillates in the bound potentials V^d_{44} and V^d_{33}, periodically exchanging amplitude between them.

The latter effect is demonstrated in Figure 5a, showing the diabatic populations $P^d_3(t)$ and $P^d_4(t)$, where

$$P^d_i(t) = \int_{z_0}^{z_{max}} \chi^d_i(z,t)^*\, \chi^d_i(z,t)\, dz \tag{4.2}$$

Similarly, the configuration space expectation value

$$\langle z^d_3(t)\rangle = \int_{z_0}^{z_{max}} \chi^d_3(z,t)^*\, z\chi^d_3(z,t)\, dz \tag{4.3}$$

is given in Figure 5b. A clear oscillation in configuration space on the lower bound potential V^d_{33} with a period of ca. 18 fs is found, while amplitude among V^d_{33} and V^d_{44} is exchanged with a

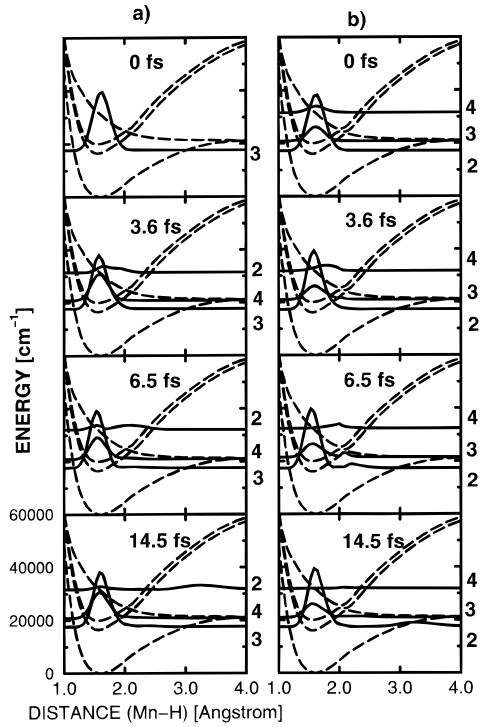

Figure 4. (a) Diabatic time evolution of the wave packets $|\chi^d_i|$ ($i = 2$, 3, 4) for the initial condition corresponding to scheme a: a part of the wave packet is transferred to the dissociative state by potential coupling, from where it dissociates. The wave packets are placed at the energies $E_i(t) = \langle\chi^d_i(z,t)|V^d_{ii} + \hat{T}_n|\chi^d_i(z,t)\rangle/\langle\chi^d_i(z,t)|\chi^d_i(z,t)\rangle$. The numbering is used to assign the individual wave packets to potentials V^d_{22}, V^d_{33}, and V^d_{44}, respectively. (b) Adiabatic time evolution of the wave packets $|\chi^a_i|$ ($i = 2$, 3, 4) after initial excitation into potential V^d_{33} (scheme a)): At $t = 0$ the wave packet is distributed on all three excited adiabatic potentials. The part on V^a_{44} dissociates, subsequently changing to V^a_{33} and V^a_{22}.

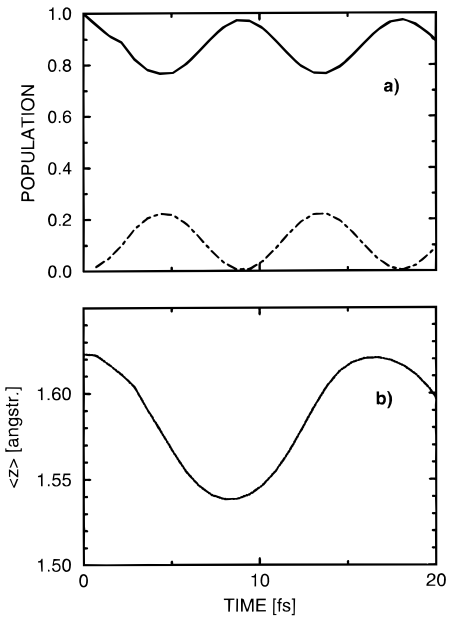

Figure 5. (a) Time evolution of the population for scheme a: $P^d_3(t)$ (solid line) and $P^d_4(t)$ (dot-dashed line). (b) Time evolution of the expectation value $\langle z^d_3(t)\rangle$ for the wave function on potential V^d_{33}.

period of 9 fs. This is explained as follows. Amplitude is transferred to the upper bound potential V^d_{44} at every time the wave packet on V^d_{33} enters the region of minimum potential energy, and hence of maximum potential coupling (see Figure

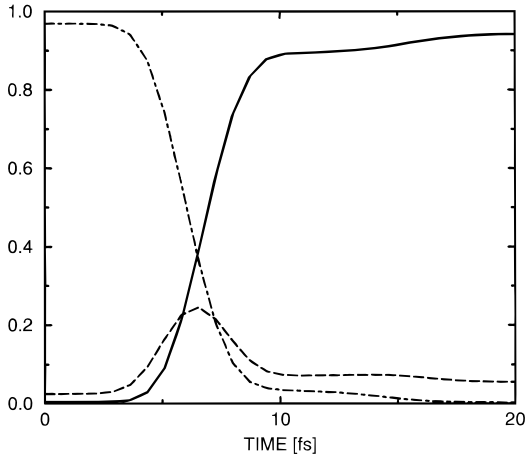

Figure 6. Time evolution of the adiabatic state populations for scheme e: $P_4^a(t)$ (dot-dashed line), $P_3^a(t)$ (dashed line), and $P_2^d(t)$ (solid line).

2c). Conversely, amplitude is lost from the upper bound to the lower bound potential when the wave packet leaves the region of large potential coupling and proceeds to the turning point in configuration space. The pronounced exchange of amplitude between the bound potentials in the diabatic representation shows that the motion of the trapped wave packet can be classified as *adiabatic*.

The corresponding time development of the wave packet $\chi^a(z,t)$ in the adiabatic representation (eq 4.1) is shown in Figure 4b. Already at $t = 0$ amplitude is found on the repulsive side of the adiabatic potential V_{44}^a. This part moves downhill and subsequently hops over to potentials V_{33}^a and V_{22}^a, as it passes the regions of the avoided crossings, where the kinetic couplings are large. The main part, however, stays trapped in the bound potentials. In the adiabatic representation, almost no amplitude is exchanged between the two lowest potentials, V_{22}^a and V_{33}^a. This supports once more the classification of the trapped dynamics as being adiabatic.

Time Evolution on the ^{3}LLCT State (σ f π^*, V_{22}^d). As a second characteristic case, the diabatic time evolution of $HMn(CO)_3(dab)$ following absorption to the lowest ^{1}LLCT excited state, and subsequent ^{1}LLCT f ^{3}LLCT intersystem crossing, is simulated according to (2.10), with the initial conditions $\chi_2^d(z,0) = \chi_{1,0}(z)$ and $\chi_3^d(z,0) = \chi_4^d(z,0) = 0$ (case e). The behavior of the wave packet (not shown here) is similar to that found in case a. Now, however, the main part dissociates.

In the adiabatic representation the main part, starting on the repulsive side of V_{44}^a, moves downhill and subsequently hops over to potentials V_{33}^a and V_{22}^a, as it passes the regions of the avoided crossings. This distinct "adiabatic surface hopping" during dissociation is characteristic for predominantly *diabatic* behavior and is demonstrated in Figure 6, where the adiabatic populations

$$P_i^a(t) = \int_{z_0}^{z_{max}} \chi_i^a(z,t)^* \, \chi_i^a(z,t) \, dz \qquad (4.4)$$

are depicted. It is also indicated how a small fraction of the total wave function is trapped.

In summary we have seen that, depending on the initial excitation into an MLCT (case a) or an LLCT state (case e), quite different dynamical results may emerge. In the former case, the excited state dynamics is predominantly adiabatic and leads to low photodissociation yields, whereas in the latter the dynamics is diabatic and the photodissociation yield is high. The question arises whether these differences have consequences also, for example, for the optical absorption spectra.

B. Electronic Absorption Spectra. As mentioned in the Introduction, we determine approximate optical absorption spectra for $HMn(CO)_3(dab)$ by simply projecting the singlet electronic ground state wave function on the triplet excited state manifold, neglecting, this way, the rapid intersystem crossing and the expected resulting spectral broadening.

The absorption spectrum $I(\omega)$ for continuous wave (CW) excitation is then obtained from the Fourier transform of an autocorrelation function $S(t)$,[23]

$$I(\omega) \propto \omega \int_{-\infty}^{\infty} dt e^{i(\hbar\omega + E_{1,0})t/\hbar} S(t) \qquad (4.5)$$

where $E_{1,0}$ is the energy of the vibrational ground state of the electronic ground state. Further,

$$S(t) = \sum_{i=2}^{4} \langle \chi_i^d(z,0) | \chi_i^d(z,t) \rangle \qquad (4.6)$$

and

$$\chi_i^d(z,0) = \chi_{1,0} \quad (i = 2, 3, 4) \qquad (4.7)$$

Note that in (4.5) and (4.7) the (diabatic) Condon approximation has been employed, which is, in view of the neglect of spin−orbit coupling, only a moderate additional assumption. It is further assumed that all triplet states are accessible by the initial excitation with equal probability. The $\chi_i^d(z,t)$ are obtained by solving the fully coupled 3×3 diabatic Schrödinger equation (2.10), with (equal) initial wave functions $\chi_i^d(z,0)$.

The computed electronic absorption spectrum shown in Figure 7a has the following features. There are several narrow peaks in the region between 15 000 and 22 000 cm^{-1}, a broad band with a maximum at above 31 000 cm^{-1}, and a fine structure superimposed to it. All peaks (including the structure on the band) occur at energies equal to the differences between the electronic ground state's vibrational ground state and the eigenenergies of the coupled bound MLCT curves and correspond to "bound−bound" transitions. The broad background in the high-energy region is caused by rapid dissociation of the wave packet on the repulsive potential, *i.e.* a "bound-free" transition. The structure superimposed to it is caused by the coupling of the free state's continuum to the bound potential and shows therefore Fano line shapes.[51]

Besides the *Fano resonances*, a second effect associated with the non-adiabatic couplings is a shift observed for the individual peaks and the broad, high-energy band. With the full 3×3 excited state coupling included, relative to the uncoupled case, the eigenvalues of the lowest MLCT state appear to be slightly shifted (about 400 cm^{-1}) to lower energies ("*red-shift*"), whereas the maximum of the broad peak originating from the dissociative state is shifted (about 400 cm^{-1}) to higher energies ("*blue-shift*"). Incidently, both red- and blue-shifts are operative in the case of the higher MLCT state V_{44}^d, leading, in effect, to an almost unshifted corresponding line spectrum.

The two mentioned coupling effectss resonance structures and line shiftss have been verified through computer experiments, in which the couplings were artificially turned off; that is, the V_{ij}^d in (2.11) were set to zero for $i \neq j$. The result is shown in Figure 7b, according to which the spectrum shows unshifted peaks and an unshifted continuum, with no structure superimposed to the latter.

Despite the simplicity of our approach, the calculated spectrum reproduces the main features of the experimental ones, recorded for the same family of complexes.[10] Accordingly, in the low-energy region (around 20 000 cm^{-1}) a strong absorption

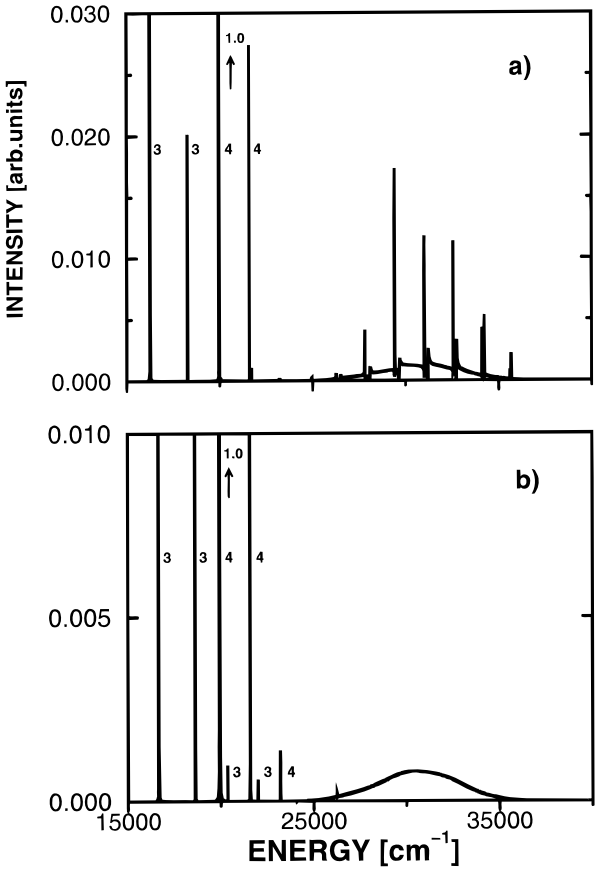

Figure 7. Simplified, theoretical electronic absorption spectra for $HMn(CO)_3(dab)$: (a) with all non-adiabatic couplings included; (b) without any couplings. Note the red-shift in the low-energy part and the blue-shift in the high-energy part if the coupling is turned on. The labels at the peaks in the low-energy region indicate transitions from V_{11}^d to the bound MLCT states V_{33}^d and V_{44}^d, respectively.

feature is observed, corresponding to different MLCT transitions. Separated from this feature, at higher energies (around 25 000 cm^{-1}) the LLCT transition sets in, resulting in a broad absorption with a low-resolution structure on top. The main difference of our theoretical spectrum from the measured ones is that the latter are broadened, particularly so in their low-energy region. This is mostly because in our treatment the fast ISC processes are not included (see above) and further (i) because other, so far undetected, MLCT states are expected in the relevant energy region, (ii) because of solvent effects, and (iii) because of other vibrational modes neglected here.

C. Photoreactivity: Cleavage of the Mn−H Bond. In this section, the photoreactivity of $HMn(CO)_3(dab)$ is investigated in some detail. For this purpose, as a measure for the efficiency of the Mn−H bond-breaking reaction, the time-dependent dissociation probability $p_{diss}(t)$ is computed for the different propagation schemes a−h alluded to earlier. These different schemes serve to systematically study the influence of the excitation wavelength, and initial vibrational excitation on the product yield, and to contribute to the understanding of the role of various excited states and the coupling between them.

The dissociation probability indicates which fraction of the wave packet has passed a certain bond distance z_{diss} at time t,

$$p_{diss}(t) = 1 - \sum_i \int_{z_0}^{z_{diss}} \chi_i^*(z,t)\, \chi_i(z,t)\, dz \qquad (4.8)$$

where the point separating bound from dissociated species is chosen as $z_{diss} = 4.022$ Å.

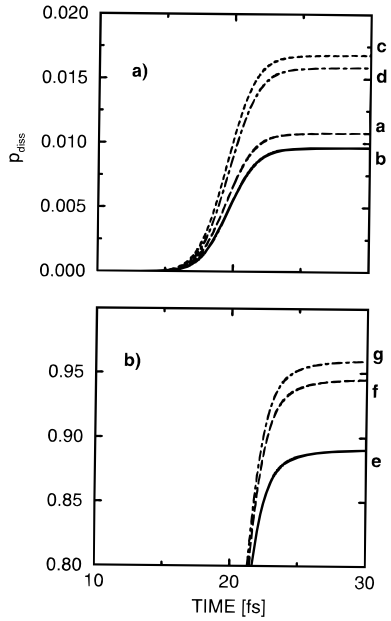

Figure 8. (a) Dissociation probabilities for excitation into an MLCT state, comparison for propagations including one or two MLCT states. (b) Dissociation probabilities for excitation into the dissociative state, comparison for propagations including one or two MLCT states. The labels at the side refer to the different schemes in Figure 3.

In Figure 8 the dissociation probabilities for the cases a−e are compared. This shows first that the dissociation probability is higher for initial excitation into the dissociative LLCT state (cases e−g) than for initial excitation to an MLCT state (cases a−d). Further, it can be seen that for excitation into the MLCT band (Figure 8a) the dissociation probability is increased if there are two MLCT states instead of only one (c > d and a > b), whereas for initial excitation to the dissociative state the dissociation probability decreases if there are two MLCT states instead of one (e < f < g).

These findings are easily interpreted. An increased number of coupled states increases the number of channels connecting the bound MLCT with the unbound LLCT PEC. Therefore, the amplitude of the wave packet will be more evenly distributed on all potentials, which leads to an increase in the dissociation probability for initial excitation to a bound MLCT state and to a decrease for initial excitation to the dissociative state. The effect is not very pronounced in the present model study, but may be more important in real complexes.

This shows that not only neglected degrees of freedom but also the coupling to many excited states lower the product yield, and hence the efficiency of various photoreaction control parameters. Nevertheless, it seems possible to achieve high dissociative product yields by using, beyond simple wavelength variation, more subtle photoreaction control strategies. One of them is vibrationally mediated chemistry (VMC),[53] where a first IR laser pulse is used to vibrationally excite a certain molecular bond, before a second, UV/vis laser beam drives the desired photoreaction.

In the present context, VMC is used to increase the dissociation probability after irradiation into the MLCT band. For this purpose, an IR photon serves to initially excite a vibrational eigenstate $\chi_{1,v}$ of the electronic ground state. Then the UV photon induces the transition to the lower bound MLCT state V_{33}^d (case h). (Again, the real excitation/ISC cascade is neglected.)

The resulting time-dependence of the dissociation probability as a function of the vibrational level v is shown in Figure 9. If we start from a vibrationally excited state $\chi_{1,v}$ with $v > 1$ and

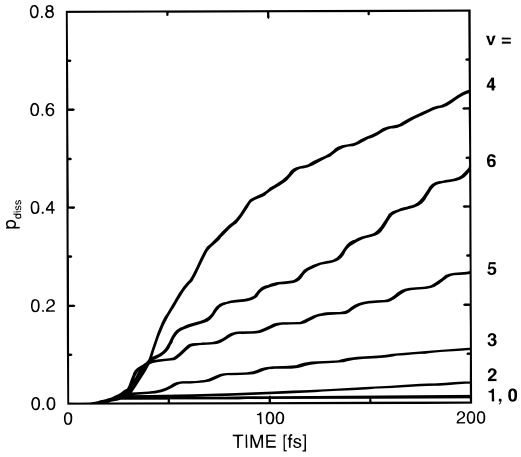

Figure 9. Dissociation probabilities after initial vibrational excitation of the ground state (scheme h). The numbers refer to the vibrational quantum number v. The dissociation probabilities increase from $v = 0$ to $v = 4$; the values for $v = 5$ and 6 are lower than for $v = 4$.

excite to the lower MLCT state V_{33}^d, the dissociation probabilities do not reach their saturation levels after 25 fs, but rather keep increasing stepwise over time. This is because the vibrationally excited molecules keep vibrating also in the bound excited state potentials and lose intensity to the unbound potential each time they pass through the regions of large potential coupling. Therefore, in Figure 9 the dissociation probabilities are terminated after 200 fs, and the effects of vibrational excitation are recorded at this time. It is found that the dissociation probability at 200 fs increases for the vibrational ground state levels $v = 1$ to $v = 4$ and then decreases for $v = 5$. Hence, vibrational excitation serves indeed to increase the product yield, but not so in a monotonic way. This can be explained by the fact that for very high v the wave packet behaves more classically, *i.e.* becomes localized closer to the classical turning points in the bound, diabatic potential. In these regions, however, the coupling between the bound and the dissociative surfaces is small, as seen in Figure 2c. Thus, less amplitude is transferred from the bound to the dissociative PEC.

V. Summary and Conclusions

In this work we have studied, using quantum mechanical first principles methods, the photochemistry and optical spectroscopy of $HMn(CO)_3(dab)$, serving as a model compound for a class of diimine complexes with novel properties. We have shown that the numerical diabatization of the three lowest electronically excited $^3A'$ potentials along the Mn−H bond direction yields "smooth" potential couplings with maxima in the ground state equilibrium region. The nuclear wave packet dynamics, performed for practical reasons in the diabatic representation of the time-dependent Schrödinger equation, can be classified as predominantly adiabatic if the initial excitation populates the MLCT band, but predominantly diabatic if the LLCT state is populated. Further, the dissociation probability is low in the first case and high in the latter. The fact that the MLCT states are found to be partially reactive is a consequence of the non-adiabatic couplings. The two excitation domains show up as two distinct absorption features in both the theoretical and experimental optical spectra. The theoretical spectrum, in which the exact nature of the excitation and ISC is neglected, appears to be more structured. It is found that non-adiabatic couplings lead to Fano resonances in the continuum part of the spectra and to red- or blue-shifts of their low- and high-energy parts, respectively. In view of the possible practical applications of the diimine complexes, we also tried to selectively control dissociation yields. It was found that the irradiation wavelength is an efficient control parameter. On the other hand, non-adiabatic couplings were found to decrease the selectivity. By using the concept of vibrationally mediated chemistry, the selectivity can be increased again, but not beyond a certain degree, which is once more determined by non-adiabatic couplings. The increase of reactivity of the MLCT by vibrational preparation is a consequence of the fact that in the adiabatic pictures the effective barriers separating bound from unbound regions are lowered if the educts are vibrationally excited.

The results for the photoreactivity of the Mn−H bond point therefore also to the importance of the relative energetic position of the bound MLCT states to the high dissociative LLCT state for this class of transition metal complexes. The latter depends on external experimental parameters, but also on the metal center, on the diimine ligand, or on ligands R other than H. The variation of these parameters can easily lead to a modification of the adiabatic energy barriers, and hence of the photoreactivity of the MLCT states.

We have also shown that it is important not only to take care of the various excited states but also to take their couplings into account. Here we have solely focused on the role of non-adiabatic couplings. However, future work should include also the excited singlet states and their spin−orbit coupling to the triplet states. This is not an easy task, but appears to be necessary to arrive at a more complete microscopic understanding of the functioning of diimine complexes. Work along these lines is in progress and has in fact also been done for other transition metal compounds.[21] Further, excited states of A″ symmetry should be included. Finally, in view of possible applications offered by the concept of the "bond selective chemistry", the inclusion of two competing reaction channels, namely, the homolytic breaking of the Mn−H bond and the heterolytic loss of CO, will be an interesting line of future research.

Acknowledgment. It is a pleasure to thank J. Manz, D. J. Stufkens, and M. C. Heitz for valuable discussions. K.F. acknowledges financial support by the Fonds der Chemischen Industrie. This work was supported by the Euronetwork "Quantum Chemistry on Transition Metal Complexes" No. ERBCHRXCT 930156. The quantum *ab initio* calculations have been carried out on the C98 computer of the IDRIS (Orsay, France) through a grant of computer time from the Conseil Scientifique.

References and Notes

(1) Kalyanasundaram, K. *Coord. Chem. Rev.* **1982**, *46*, 159, and references therein.
(2) Meyer, T. J. *Pure Appl. Chem.* **1986**, *58*, 1193.
(3) Meyer, T. J. *Acc. Chem. Res.* **1989**, *22*, 163.
(4) Juris, A.; Balzani, V.; Barigelletti, F.; Campagna, S.; Belser, P.; von Zelewsky, A. *Coord. Chem. Rev.* **1988**, *84*, 85.
(5) Krausz, E.; Ferguson, J. *J. Prog. Inorg. Chem.* **1989**, *37*, 293.
(6) Stufkens, D. J. *Comments Inorg. Chem.* **1992**, *13*, 293.
(7) Balzani, V.; De Cola, L.; Prodi, L.; Scandola, F. *Pure Appl. Chem.* **1990**, *62*, 1457.
(8) Scandola, F.; Bignozzi, C. A.; Chiorboli, C.; Indelli, M. T.; Rampi, M. A. *Coord. Chem. Rev.* **1990**, *97*, 299.
(9) Juris, A.; Campagna, S.; Bidd, I.; Lehn, J. M.; Ziessel, R. *Inorg. Chem.* **1988**, *27*, 4007.
(10) Stufkens, D. J. *Coord. Chem. Rev.* **1990**, *104*, 39, and references therein.
(11) Meyer, T. J.; Caspar, V. *Chem. Rev.* **1985**, *85*, 187.
(12) Rossenaar, B. D.; Kleverlaan, C. J.; Stufkens, D. J.; Oskam, A. *J. Chem. Soc., Chem. Commun.* **1994**, 63.
(13) Rossenaar, B. D.; van der Graaf, T.; van Eldik, R.; Langford, C. H.; Stufkens, D. J.; Vleck, A. *Inorg. Chem.* **1994**, *33*, 2865.

(14) Stor, G. J.; Stufkens, D. J.; Vernoojis, P.; Baerends, E. J.; Fraanje, J.; Goubitz, K. *Inorg. Chem.* **1995**, *34*, 1558.
(15) Veillard, A.; Strich, A. *J. Am. Chem. Soc.* **1988**, *110*, 3793.
(16) Daniel, C. *J. Phys. Chem.* **1991**, *95*, 2394.
(17) Daniel, C. *J. Am. Chem. Soc.* **1992**, *114*, 1625.
(18) Daniel, C.; Veillard, A. *Theoretical Studies of the Photochemistry of Transition Metal Hydrides*; Dedieu, A., Ed.; VCH: New York, 1991; pp 235−261.
(19) Daniel, C.; Heitz, M. C.; Lehr, L.; Manz, J.; Schröder, T. *J. Phys. Chem.* **1993**, *97*, 12485.
(20) Daniel, C.; Heitz, M. C.; Lehr, L.; Schröder, T.; Warmuth, B. *Int. J. Quantum Chem.* **1994**, *52*, 71.
(21) Daniel, C.; Heitz, M. C.; Manz, J. Ribbing, C. *J. Chem. Phys.* **1995**, *102*, 905.
(22) Daniel, C.; Kolba, E.; Lehr, L.; Manz, J.; Schröder, T. *J. Chem. Phys.* **1994**, *98*, 9823.
(23) Heller, E. J. *Acc. Chem. Res.* **1981**, *14*, 368.
(24) Schinke, R. *Photodissociation Dynamics*; Cambridge University Press: New York, 1993; pp 72−75, 355.
(25) Finger, K.; Daniel, C. *J. Chem. Soc., Chem. Commun.* **1995**, 1427.
(26) Werner, H. J.; Meyer, W. *J. Chem. Phys.* **1981**, *74*, 5802.
(27) Heumann, B.; Weide, K.; Düren, R.; Schinke, R. *J. Chem. Phys.* **1993**, *98*, 5508.
(28) Domcke, W.; Woywood, C.; Stengle, M. *Chem. Phys. Lett.* **1994**, *226*, 257.
(29) Neuheuser, T.; Sukumar, N.; Peyerimhoff, S. D. *Chem. Phys.* **1995**, *194*, 45.
(30) Gu, J. P.; Buenker, R. J.; Hirsch, G.; Kimura, M. *J. Chem. Phys.* **1995**, *102*, 7540.
(31) Kolbuszewski, M.; Wright, J. S.; Buenker, R. J. *J. Chem. Phys.* **1995**, *102*, 7519.
(32) Heltema, H.; Yarkony, D. R. *J. Chem. Phys.* **1995**, *102*, 8431.
(33) (a) Manthe, U.; Köppel, H. *J. Chem. Phys.* **1990**, *93*, 345. (b) Manthe, U.; Köppel, H. *J. Chem. Phys.* **1990**, *93*, 1658. (c) Manthe, U.; Köppel, H.; Cederbaum, L. S. *J. Chem. Phys.* **1991**, *95*, 1708.
(34) Köppel, H. *Chem. Phys.* **1983**, *77*, 359.
(35) Schneider, R.; Domcke, W. *Chem. Phys. Lett.* **1989**, *159*, 61.
(36) Schneider, R.; Domcke, W.; Köppel, H. *J. Chem. Phys.* **1990**, *92*, 1045.
(37) van Dishoeck, E. F.; van Hemert, M. C.; Allison, A. C.; Dalgarno, A. *J. Chem. Phys.* **1984**, *81*, 5709.
(38) Reber, C.; Zink, J. *J. Chem. Phys.* **1992**, *96*, 2681.
(39) Engel, V.; Metiu, H. *J. Chem. Phys.* **1989**, *90*, 6116.
(40) Rossenaar, B. Ph.D. Thesis, Amsterdam, 1995.
(41) Smith, F. T. *Phys. Rev.* **1969**, *179*, 111.
(42) Siegbahn, P. E. M.; Almlof, J.; Heiberg, A.; Roos, B. O. *J. Chem. Phys.* **1981**, *74*, 2384.
(43) Siegbahn, P. E. M. *Int. J. Quantum Chem.* **1983**, *23*, 1869.
(44) Saalfrank, P. *Chem. Phys.* **1995**, *193*, 119. We note that the algorithm for the calculation of the transformation matrix $\underline{\underline{U}}$ requires the use of a small grid spacing Δz compared to the hwhm of the $T_{ij}^{(1)}$, and simultaneously a long grid z_{max}. Then the narrow kinetic couplings can be well represented, and the boundary condition (2.6) is fulfilled. The shape of the diabatic curves and potential couplings if found to be sufficiently converged with a grid length of $z_{max} = 26.459$ Å and a spacing $\Delta z = 5.29 \times 10^{-1}$ Å.
(45) Hirsch, G.; Bruna, P. J.; Buenker, R. J.; Peyerimhoff, S. D. *Chem. Phys.* **1980**, *45*, 335.
(46) Heitz, M. C. Private Communication, 1995.
(47) Meyer, R. *J. Chem. Phys.* **1969**, *52*, 2053. Marston, C. C.; Balint-Kurti, C. G. *J. Chem. Phys.* **1989**, *91*, 3571.
(48) Kosloff, R.; Kosloff, D. *J. Chem. Phys.* **1983**, *79*, 1823. Kosloff, R. *Ann. Rev. Phys. Chem.* **1994**, *45*, 145.
(49) Kosloff, R. *J. Phys. Chem.* **1988**, *92*, 2087.
(50) Bisseling, R. H.; Kosloff, R.; Manz, J. *J. Chem. Phys.* **1985**, *83*, 993.
(51) Fano, U. *Phys. Rev.* **1961**, *124*, 1866. Fano, U.; Cooper, J. W. *Phys. Rev. A* **1965**, *137*, 1364.
(52) Stufkens, D. J. Private Communication, 1995.
(53) Crim, F. F. *Science* **1990**, *249*, 1387. Imre, D. G.; Zhang, J. *Chem. Phys.* **1989**, *139*, 89.
(54) Schmidt, G. S.; Paulus, H.; van Eldick, R.; Elias, H. *Inorg. Chem.* **1988**, *27*, 3211.
(55) McNeill, E. A.; Scholer, F. R. *J. Am. Chem. Soc.* **1977**, *99*, 6243.

JP952497I